Numerical Methods in Civil Engineering

Journal Homepage: https://nmce.kntu.ac.ir/

Numerical investigation of GFRP bars contribution on performance of concrete structural elements

Pegah Aghabozorgi*, Alireza Khaloo, Sina Hassanpour*****

ARTICLE INFO

RESEARCH PAPER

Article history:
Received:
December 2020,
Revised:
February 2021,
Accepted:
April 2021.

Keywords:
Beams, Columns, GFRP bars, Compressive reinforcement, Finite Element Methods, Modelling, Structural Analysis

Abstract:

In this study, twenty glass fiber reinforced polymer (GFRP) reinforced concrete specimens were modelled using finite element method to predict the effect of GFRP compressive bars on the flexural strength and ductility of GFRP reinforced concrete beams. Also, the contribution of GFRP longitudinal rebars to the load-carrying capacity of reinforced concrete columns is determined. The concrete elastoplastic behaviour after the peak load was defined using the concrete damaged plasticity model in ABAQUS software. The FE results were validated using the experimental data reported in the literature. The results demonstrated a close agreement between the load-displacement curves obtained from numerical analysis and the tests. An increase in the percentage of GFRP compressive reinforcement resulted in slightly higher energy absorption and ductility in the GFRP concrete beams. According to the FE analysis, increasing GFRP compressive reinforcement has a minor influence on the flexural strength of beams. Moreover, decreasing the percentage of longitudinal reinforcement leads to a reduction in the strength and ductility of columns, and higher loss in strength was observed when greater eccentricity was applied in columns.

1. Introduction

Fiber-reinforced polymer (FRP) bars have recently emerged as an alternative reinforcement over conventional steel bars for concrete structures in harsh environments due to overcoming corrosion and other problems commonly associated with steel reinforcement. GFRP (Glass Fiber Reinforced Polymer), CFRP (Carbon Fiber Reinforced Polymer), and AFRP (Aramid Fiber Reinforced Polymer) are the most commonly used FRPs. In recent studies, GFRP is considered as a feasible replacement for steel due to its relatively low cost and high tensile strength compared to the other commercially available FRPs [1]. Corrosion of steel reinforcement due to saltwater and harsh marine environments can lead to deterioration (loss in strength and serviceability) of the reinforced concrete (RC) structures; thus, corrosion-resistant bars have been utilized as a way to improve serviceability and lengthen lifetime of many concrete structures worldwide [2].

* *Graduate student, Department of Civil Engineering, Sharif University of Technology, Tehran, Iran.*
** *Corresponding Author: Distinguished Professor, Department of Civil Engineering, Sharif University of Technology, Tehran, Iran, Email: Khaloo@sharif.edu*
*** *Graduate student, Department of Civil Engineering, Sharif University of Technology, Tehran, Iran.*

Furthermore, non-conductive and non-magnetic properties of FRP reinforcement make them applicable for use in equipment sensitive to electromagnetic fields and buildings which host magnetic resonance imaging (MRI) units [3].

Due to some properties of FRP materials such as low elastic modulus and the linear behaviour without yield point, the maximum contribution of compression FRP bars in pure axially loaded columns at ultimate concrete strain (typically $\boldsymbol{\varepsilon_{cu}}$=0.003) is expected to be small; as a result, different design provisions to analyze concrete members reinforced with FRP under different loading conditions is required to consider the differences in the mechanical properties of the steel and GFRP materials. Thus, several studies have been performed regarding the modelling and implementation of GFRP in structural elements [4-8]. Although the effective role of GFRP rebars in the compression member capacity calculations is highlighted in a number of recent studies, the current design codes such as ACI 440.1R-15 [9], CAN/CSA S806-02 [10],TR55 [11], ISO 10406-01 [12], and fib [13] do not recommend the use of FRP bars as longitudinal reinforcement in columns. However, some studies reported that not only is the exclusion of stiffness and compressive strength of GFRP reinforcement conservative, but the GFRP compressive strength results are also in better agreement

with theoretical capacities and experimental data [13-16]. In this regard, carrying out numerical simulations along with laboratory studies is necessary to provide more accurate evaluation of the FRP performance on reinforced concrete structural members and develop new rules in the design of FRP reinforced structures.

The importance of identifying the behaviour of FRP bars in compression members as well as their favorable performance as flexural tension reinforcement have been highlighted in the past studies. Deitz et al. suggested ultimate compressive strength of non-slender short GFRP bars to be approximately 50% of their tensile strength, whereas the elastic modulus in compression was found to be the same as in tension [17]. On the other hand, a study carried out by Afifi et al. [18], [19] attributed lower ultimate compressive strength to GFRP rebars (approximately 35% of their ultimate tensile strength) than that measured by Deitz et al. [17]. Due to the relatively low elastic modulus of GFRP bars, they are required to be well confined with stirrups in order to safely sustain some buckling [20]. This fact was also confirmed by the results of investigations attributing low ultimate capacity, low ductility, and brittle failure mode to columns with large tie spacing [21], [22]. There are also studies that have been successful in providing some insight into the behaviour of FRP-RC columns under various loading conditions. Alsayed et al. [23] set up an experiment to compare the effect of using GFRP ties on axial capacity of concentrically loaded RC columns compared to using steel ties. The results showed a reduction up to 10% in axial capacity of GFRP reinforced columns compared to those reinforced with steel ties. Accordingly, the failure modes are more abrupt for columns reinforced with GFRP ties than those reinforced with steel ties [2], [18], [19], [21]. Another study completed by Mirmiran et al. [24] indicated that FRP reinforced concrete columns are more susceptible to the length effects due to lower elastic modulus of FRP rebars. The study also proposed a reduction in slenderness limits of 22% for steel-reinforced columns and 17% for FRP-reinforced columns while maintaining a minimum reinforcement ration of 1%.

Choo et al. [25] investigated the minimum FRP reinforcement ratio required for rectangular columns subjected to pure bending by presenting a set of equations in order to prevent the tensile failure of FRP rebars. They also found that the brittle nature of GFRP rebars makes GFRP-reinforced members essential to be overly reinforced. Sharma et al. [26] compared the axial load capacities of three GFRP-RC columns with three different reinforcement ratios: 0.723, 1.08, and 1.45% and concluded that increasing the reinforcement ratios is followed by increasing the ductility of columns. In spite of some emphasis on the prediction of the behaviours of GFRP-RC columns using existing design guides for steel reinforcement, Elchalakani et al. [14] investigated interaction diagrams of these columns and found no distinct balanced failure point on them for longitudinal reinforcement ratios above 3%. Further studies on concrete columns reinforced with GFRP bars showed an average 3%-4% increase in load carrying capacity of GFRP-reinforced concrete columns compared to their corresponding plain concrete columns when stress block depth coefficient was equal to 1.0.

The improvement in terms of load capacity was achieved through decreasing stirrups spacing [27-29]. Moreover, GFRP-RC columns, which are exposed to large eccentricities experienced significant reduction in their ultimate load capacity caused by the non-uniform stress contribution [30]. Also, a number of numerical studies have simulated GFRP reinforced concrete columns and beams using three-dimensional finite-element analysis (FEA) in ABAQUS to predict post-peak responses and the degraded stiffness of cracked concrete through modified concrete damage plasticity (CDP) model [31-34]. Amiri et al. [35] predicted the flexural response of a reinforced Geopolymer concrete beam using FEA in ABAQUS software. They compared the results from FEA to the experimental results, and observed some differences in the deflections of beams while a good agreement was found between their crack patterns. In a research carried out by Ibrahim et al. [36] the same elastic modulus was applied for GFRP rebars, whether in tension or compression, using a linear-strain relationship. Aliasghar-Mamaghani et al. [37] investigated the seismic behaviour of RC frames reinforced with GFRP bars by considering moment-curvature diagrams for beam and column sections at plastic hinge regions. Their study resulted in higher strength with an average of 13% for frames reinforced with GFRP bars as compared to similar frames reinforced with steel bars under seismic loading. The dynamic performance of concrete slabs reinforced with GFRP and steel bars subjected to impact loading was investigated by Sadraie et al. [38] The slabs reinforced with GFRP bars provided slightly less resistance and higher displacement than that reinforced with steel bars, and adjusting the amount and arrangement of GFRP bars led to better performance in GFRP slabs.

1.1 Research Significance

The above-mentioned investigations highlight the necessity of further numerical and experimental studies on the GFRP-RC columns and beam columns under combined loading conditions to be able to fully address the structural design of concrete members reinforced with GFRP bars. Therefore, this research is carried out to take a step toward this objective using a FEA model by selecting appropriate factors such as mesh size and confinement model, and verify the model with experimental data. In addition, the load-moment interaction

diagrams, obtained from the tests and the finite element analysis, are presented and thoroughly compared with each other. The study described in this paper involves numerical simulations of twenty GFRP reinforced concrete specimens subjected to various loading conditions in order to predict the effect of GFRP compressive bars on the flexural strength and ductility of GFRP reinforced concrete beams, and the contribution of GFRP longitudinal bars on the capacity of reinforced concrete columns.

2. Test model specimens

One of the most referred literatures to experimental data on beams and columns belongs to Elchalakani et al. [39]. Therefore, the verification of finite element models is based on their test specimens' geometry and material properties. For numerical simulation through FE method, a cross sectional area of 120*160 mm^2 and a length of 1101 mm are chosen for both eight reinforced concrete column specimens and twelve reinforced concrete beam specimens, considering eccentricity and four-point bending loading, respectively, in ABAQUS software. Fig. 1 shows geometry of cross-section and details of reinforcement required for the FE model of both the beams and the columns which are designed for verification in ABAQUS software. Furthermore, the schematic drawings of concrete beams and columns and the test setup are shown in Fig. **2** Concrete specimens are longitudinally and transversely reinforced with GFRP bars. GFRP-RC specimens are reinforced with six No. 4 (12.7mm) longitudinal rebars, providing a longitudinal reinforcement ratio of 1.83% and also reinforced with No. 2 (6.35 mm) stirrups at 150mm spacing. The arrangement of stirrup spacing is in accordance with ACI code [9] provisions. Also, concrete cover for GFRP-RC specimens is equal to 20mm as shown in Fig. 1.

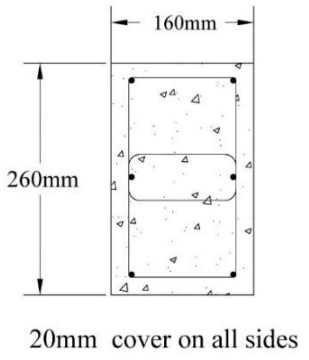

Fig. 1: A schematic of cross section and reinforcement arrangement [39].

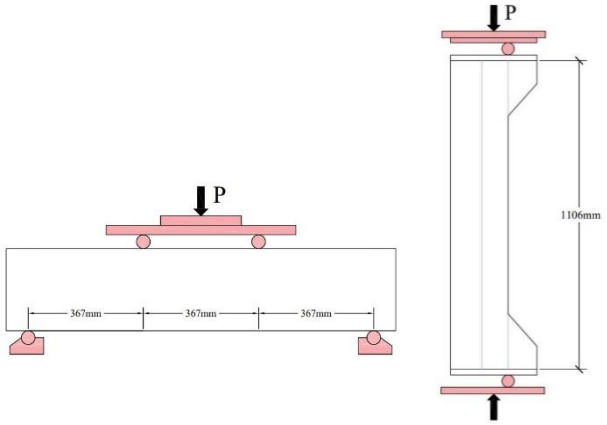

(a) (b)

Fig. 2: The general test setup for (a) GFRP reinforced concrete beam (b) GFRP reinforced concrete column[39]

Table. 1 lists the physical properties of the GFRP bars used in the specimens and compressive strength $\acute{f}_c$ of 32.75MPa is considered for concrete in calculations.

Table. 1: Physical properties of GFRP bars [40]–[42]

Bar size	Diameter (mm)	Area (mm^2)	Tensile elastic modulus (Gpa)	Ultimate strength (MPa)	Tensile strength (MPa)	Ultimate strain in tension (%)
#2	6.35	31.7	46.1	1.9	784	1.9
#4	12.7	126.7	46.3	1.7	708	1.7

Table. 2: Mechanical properties of column and beam specimens

Specimens	Bar diameter in compression (mm)	Bar diameter in tension (mm)	$(\frac{\rho}{\rho_{fb}})$	$(\acute{\rho})$	Bar Diameter in Stirrups (mm)	Eccentricity (mm)
GB1-1.8-F	14.225	14.225	1.8	1.146	6.35	-
GB0.5-1.8-F	10	14.225	1.8	0.573	6.35	-
GB0-1.8-F	0	14.225	1.8	0	6.35	-
GB1-1.434-F	12.7	12.7	1.434	0.9135	6.35	-
GB0.5-1.434-F	8.98	12.7	1.434	0.4567	6.35	-
GB0-1.434-F	0	12.7	1.434	0	6.35	-
GB1-1.162-F	11.43	11.43	1.162	0.7399	6.35	-
GB0.5-1.162-F	8.08	11.43	1.162	0.3699	6.35	-
GB0-1.162-F	0	11.43	1.162	0	6.35	-
GB1-0.8-F	9.52	9.52	0.8	0.5144	6.35	-
GB0.5-0.8-F	6.738	9.52	0.8	0.2572	6.35	-
GB0-0.8-F	0	9.52	0.8	0	6.35	-
GC1-1.434-25	12.7	12.7	1.434	0.913	6.35	25
GC1-1.162-25	11.43	11.43	1.162	0.739	6.35	25
GC1-0.8-25	9.48	9.48	0.8	0.5	6.35	25

GC1-1.8-25	14.225	14.225	1.8	0.573	6.35	25
GC1-1.434-45	12.7	12.7	1.434	0.913	6.35	45
GC1-1.162-45	11.43	11.43	1.162	0.739	6.35	45
GC1-0.8-45	9.48	9.48	0.8	0.5	6.35	45
GC1-1.8-45	14.225	14.225	1.8	0.573	6.35	45

In this paper, 20 concrete specimens are modelled in the ABAQUS software, three of which are verified with empirical results, and the rest are built in the software for further behaviour evaluation. The failure type including concrete crushing and reinforcement rupture is considered as a criterion for ending the analysis. For beams, the loading is applied under displacement control regime through which a displacement of 50mm is applied on two symmetric lines spaced 367mm apart, while for columns, a displacement of 15mm at desired eccentricity is applied at the center of the steel plate tied on top of the column. The eccentricity is applied around the weak axis to prevent lateral buckling. The specimens are analyzed under static loading. Table. 2 shows the mechanical properties of all the specimens modelled in the software. According to Table. 2, the first two letters in each specimen denotes the type of tested specimen, where "GB" represents GFRP beam and "GC" represents GFRP column. The number after the initial two letters denotes the ratio of compression reinforcement to FRP reinforcement, with the amounts of 1, 0.5, and 0, respectively, indicating equal and half amount of the FRP reinforcement, without compression reinforcement. The latter number denotes the ratio of FRP reinforcement to the balance reinforcement ($\frac{\rho}{\rho_{fb}}$). Finally, the last letter or number after the dash denotes the test method, where "F" represents flexural loading in the four-point bending test and the number represents the load eccentricity in eccentric loading of column.

3. Finite Element Simulations

3.1 Methodology

The concrete specimens are modelled as homogenous three-dimensional solid sections whereas, the longitudinal and transverse reinforcement are simulated as three-dimensional wire elements. The element type defined for concrete is C3D8R, which is a three-dimensional eight-noded hexahedral element with reduced integration and suitable for nonlinear static and dynamic analyses. Moreover, the element type defined for reinforcement is considered to be T3D2R, which is a deformable two-noded truss element; the main reason of using the truss element for GFRP reinforcement is to provide only axial stiffness in return for the weak strength of GFRP materials in the direction perpendicular to their grain direction. The typical geometry of FE model of concrete beam and eccentrically loaded column are shown in Fig. **3**. It should be noted that half of the beam is modelled in the ABAQUS software due to symmetry.

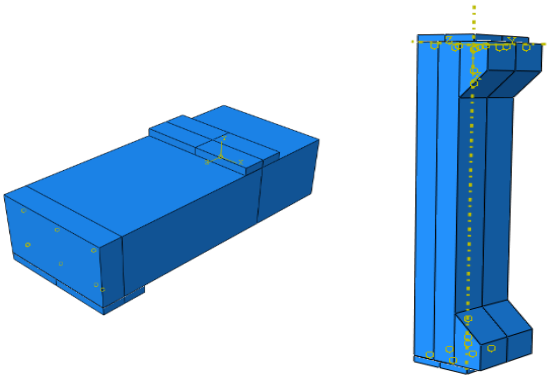

(a) (b)

Fig. 3: The typical geometry of the FE models of (a) concrete beams, (b) eccentrically loaded columns

In this study, the concrete damage plasticity model is selected to model non-linear behaviour of concrete based on two fracture mechanisms: tensile cracking and compressive crushing. The embedded constraint is imposed to simulate the interaction between the rebars and the surrounding concrete. In fact, the approach applied in this constraint restricts the rebars nodes to their corresponding freedom degree in the host domain. Thus, instead of simulating the interaction between the concrete and the reinforcement, the bars and stirrups are embedded in the concrete that will lead to adjoining the reinforcement bars to their neighbouring space and their uniform movement. Also, the bars slippage in the concrete is not considered. Furthermore, the steel plates are tied to the top and bottom surfaces of columns which distribute the load on the column. As a result of the definition of tie constraint between the surface of concrete and the steel plate, their freedom degrees are connected to each other in order to prevent the slipping of steel plate on concrete surface. All concrete specimens are meshed with an approximate size of 40mm in three directions (longitudinal, transverse, and thickness).

3.2 Material Modelling

3.2.1 Concrete Model

There is a wide spectrum of inelastic behavioural characteristics to be defined in ABAQUS software among which concrete damage plasticity (CDP) model based on the study carried out by Liu et al. [43] is selected as the most appropriate model to describe the nonlinear behaviour of concrete material [44]. The basis of this model is the

definition of two fracture mechanisms, tensile cracking and compressive crushing for concrete [45]. The behaviour of concrete is divided into two separate regimes: a linear elastic behaviour in the reversible regime and a damaged plasticity behaviour in the irreversible regime. The Young's modulus of concrete in the linear elastic region is specified using Eq. (1) from ACI363R-92 [46].

$$E_C = 3320\sqrt{f_c'} + 6900 \quad (1)$$

Where f_c' is the compressive strength of the concrete. The Poisson's ratio is considered as 0.2 for concrete.

The concrete damaged plasticity model is introduced to model the behaviour of reinforced concrete in the irreversible regime which compasses five behavioural components; including plasticity, compressive and tensile behaviour, confinement, and damage mechanics. In this study, the plasticity behaviour is defined as follows [47]–[50]:

$$\psi = 40 \quad (2)$$

$$\frac{f_{bo}}{f_c'} = 1.5\left(f_c'\right)^{-0.075} \quad (3)$$

$$K_c = \frac{5.5}{5 + 2\left(f_c'\right)^{-0.075}} \quad (4)$$

Where ψ is the dilation angle, a measurement of the plastic volume deformation, recommended to be in the range of 30°-40° for concrete [51], K_C is shape factor for yield surface, and f_{bo} is the initial equi-biaxial compressive yield stress. The uniaxial compressive strain-stress relationships of concrete are similarly introduced according to Relations (5), (6), (7), and (8). These equations are based on the relationships expressed by Liu et al. [43] to model stress-strain behaviour of concrete.

$$\sigma_c = \frac{E_c \times \varepsilon_c}{1 + \left((R + R_e - 2)\times\left(\frac{\varepsilon_c}{\varepsilon_{co}}\right)\right) - \left((2R-1)\times\left(\frac{\varepsilon_c}{\varepsilon_{co}}\right)^2\right) + \left(R\times\left(\frac{\varepsilon_c}{\varepsilon_{co}}\right)^3\right)} \quad (5)$$

$$R = \left(\frac{R_e}{3}\right) - 0.25 \quad (6)$$

$$R_e = \left(\frac{E_c}{E_o}\right) \quad (7)$$

$$E_o = \left(\frac{f_c'}{\varepsilon_{co}}\right) \quad (8)$$

Where σ_C is the compressive stress, ε_c is the compressive strain, and ε_{co} is the compressive strain at peak load, which is taken as 0.002 as per the recommendation by Mander et al. [52].

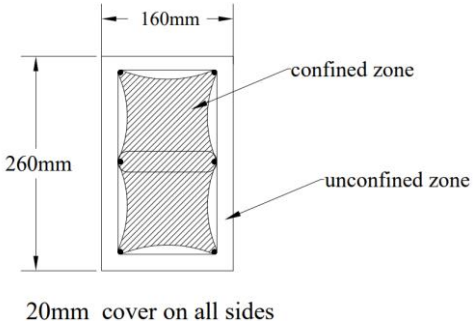

Fig. 4: Fully confined and unconfined parts at the model cross-section

In order to apply the confining effects to eccentrically loaded columns, the concrete section of column is divided into confined and unconfined parts according to Fig. **4**, and different properties are assigned to each part based on the models presented by Kappos and Konstantinidis [53] and Liu et al. [43]. The equations represented below are derived from the confinement model developed by Kappos and Konstantinidis [53] to describe the enhancement in concrete strength due to confinement provided by stirrups:

$$f_{cc}' = 0.85\times f_c' + 10.3\times\left(\alpha\times\rho_h\times f_{yh}\right)^{0.4} \quad (9)$$

Where f_{cc}' is the confined concrete strength, f_c' is the unconfined concrete strength from the cylinder, and ρ_h is volumetric ratio of the stirrups' arrangement, which can be expressed as follows.

$$\rho_h = \frac{2\left(b_c + 2d_c\right)\times A_{SP}}{b_c \times d_c \times S} \quad (10)$$

$$\alpha = \left\{1 - \frac{\Sigma_{i=1}^{n} C_i^{\,2}}{6\times b_c \times d_c}\right\}\times\left(1 - \frac{S}{2b_c}\right)\times\left(1 - \frac{S}{2d_c}\right) \quad (11)$$

In above equations, S represents the clear vertical spacing between the hoop bars, A_{SP} represents the cross sectional area of shear reinforcement, C_i represents centre-to-centre distance between laterally supported longitudinal bars, b_C and d_C are equal to the width and depth of confined concrete core, respectively, and f_{yh} is the tensile strength of GFRP ties that is calculated according to ACI-440-R-15 as:

$$f_{yh} = f_{fu}\left(0.05\frac{r_b}{d_b} + 0.3\right) \le f_{fu} \quad (12)$$

Where r_b and d_c are, respectively, the radius and diameter of the hoop bars.

The tensile behaviour of concrete, similarly to compressive, is separated into elastic and inelastic regions. The tensile yield stress is introduced in the software according to the following equation [54]:

$$f_{ct} = 0.4\sqrt{f_c'} \tag{13}$$

Also, f_t in Eq.(14) defines the tensile stress which is established by Stoner et al. [55].

$$f_t = \begin{cases} E_{co}\,\varepsilon_t & f\ \varepsilon_t < \varepsilon_{to} \\ f_{ct}\left(\dfrac{\varepsilon_{to}}{\varepsilon_t}\right)^{0.4} & If\ \varepsilon_{to} < \varepsilon_t \end{cases} \tag{14}$$

Where ε_t is tensile strain, and ε_{to} represents tensile strain at peak load. The stress-strain curves for concrete both in compression and tension are shown in Fig. **5** and Fig. **6**, respectively. As mentioned earlier, the stress-strain curve for unconfined concrete in compression is based on the relationships developed by Liu et al. [43], and that for confined concrete is obtained from the Kappos and Konstantinidis [53] confined concrete model. The linear relationship defined by Kent and Park [56] determines the values of stress and strain for concrete in tension. Furthermore, the stress values are introduced into the software in terms of inelastic strain as given in Eq.(16).

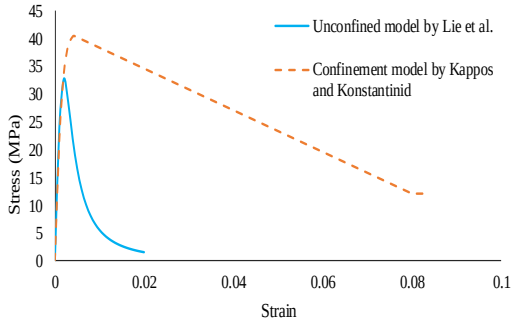

Fig. 5: The stress-strain model for confined and unconfined concrete.

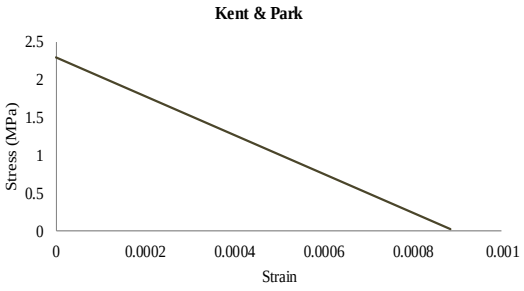

Fig. 6: The stress-strain model for concrete in tension.

The damage mechanism of concrete is another characteristic of the CDP model being applied to describe the nonlinear behaviour of reinforced concrete. The damage parameter under compressive loading, d_c and under tensile loading, d_t can be approximated as [43]:

$$d_c = \frac{\left(1-\eta_c\right)\varepsilon^{in}E_0}{\sigma_c + \left(1-\eta_c\right)\varepsilon^{in}E_0} \tag{15}$$

It should be mentioned that the plastic strain values in hardening regime (the post-yield area, where the increase in strength is invariably accompanied by plastic deformation of concrete) are calculated using the relationship defined in Eq.(16) by Liu et al. [43].

$$\varepsilon^{in} = \varepsilon_c - \varepsilon^{el} \tag{16}$$

$$\varepsilon^{pl} = \varepsilon^{in} - \frac{d_c}{\left(1-d_c\right)}\frac{\sigma_c}{E_0} \tag{17}$$

Where ε^{el}, ε^{in}, and ε^{pl} represent the elastic, inelastic, and plastic strain components, respectively.

$$\eta_c = \frac{\varepsilon^{pl}}{\varepsilon^{in}} \tag{18}$$

$$\varepsilon^{in} = \varepsilon_c - \frac{\sigma_c}{E_0} \tag{19}$$

$$d_t = \frac{\eta_t \varepsilon^{in} E_0}{\sigma_c + \eta_t \varepsilon^{in} E_0} \tag{20}$$

Where η_t and η_c can be taken as 0.6 and 0.7, respectively.

3.2.2 GFRP bar Model

The stress-strain model for the GFRP is assumed isotropic, linear elastic, and without any damage criterion. In addition, Young's modulus in tension and compression is assumed to be the same, and the compressive strength is equal to the half of tensile strength according to the previous studies [27], [40], [41]. Thus, the properties of these bars are dependent on mode loading, being either compressive or tensile. Also, Poisson's ratio is taken as 0.25. Fig. **7** illustrates the linear stress-strain curve for GFRP materials. As observed in the figure, the curve has experienced the brittle failure after yielding without entering the plastic deformation zone.

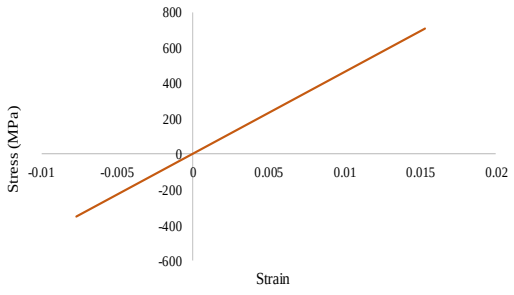

Fig. 7: The elastic stress- strain relationship of the GFRP longitudinal reinforcement [14].

4. Validation with experimental results

The predictions of finite-element models obtained from FE analysis are compared with empirical results reported by Elchalakani et al. [39]. The behaviour of flexural specimens,

and the acceptable agreement between the experimental curves and numerical load-displacement responses are shown in Fig. 8 and Fig. 9. The axial load represents support reaction force and the displacement denotes the mid-span deflection for beams and column drift. As observed in these figures, the finite element results are in close agreement with the behaviour of the two GFRP-RC columns loaded eccentrically and GFRP-RC beam under four-point bending in the ascending range of curve including the stiffness and also the peak load. However, according to Fig. 8, the load capacity of the columns at the peak loads is somewhat underpredicted by FE model, and the average difference between the peak load of FE curve and experimental curve is calculated as 5.87%. The FE load-deflection curve has been also able to predict the sudden collapse of the column with small eccentricity (25mm). But as the eccentricity increases, the accuracy of the FE simulations in predicting the behavior of test specimens decreases significantly. The sudden collapse is not modelled by the FEA for the column with high eccentricity of 45 mm but instead a gradual loss of capacity can be noticed in the FE load-deflection curves. This is probably because they were not influenced by the FRP rupture and the trend CDP model used in predicting the degradation in post peak strength, considering a loss in strength while bearing load even after cracking.

There are two distinct peaks in the experimental load-deflection curve of beams in which the second peak has higher flexural capacity than the first one, indicating higher ductility for GFRP-RC beams after initial peak. The failure which occurred after the first peak is caused by concrete crushing in compressive face that is not exactly modelled in the FE curve. Instead, the damage induced by the first failure led the load to increase at a slightly lower rate. Moreover, a small difference (about 4.1%) between the second peak load of experimental curve and of FE curve is observed, and FE curve has successfully identified the correct deflection at the peak load for GB1-1.434-F.

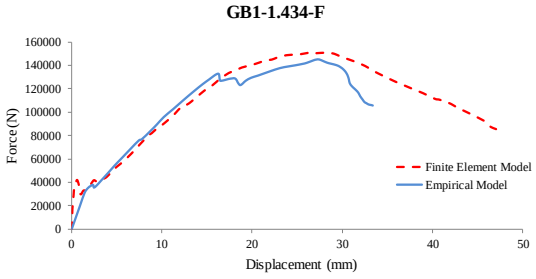

Fig. 8: Comparison of empirical and Finite Element results of axial load-deflection curve for the GFRP-RC beam (GB1-1.434-F).

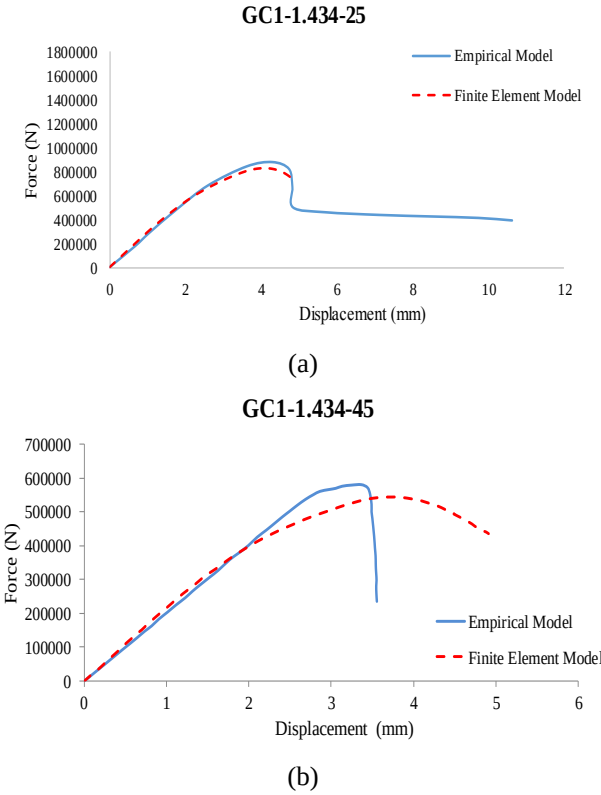

Fig. 9: Comparison of empirical and Finite Element results of axial load-displacement curves for the columns loaded eccentrically (GC1-1.434-25), (GC1-1.434-45).

Fig. 11 and Fig. 12 represent compressive damage contour of GFRP-RC columns and beam induced from Finite Element (FE) results and the failure mode of the corresponding specimens built in the laboratory from previous tests [39]. As shown in Fig. 11, the beam specimen experienced concrete crushing failure. The simulated model also properly predicted the concrete crushing in the mid-span, similar to its experimental counterpart, while the sudden collapse of the entire column caused due to concrete crushing in the compression face is listed as the failure mode of eccentrically loaded columns. Accordingly, the results showed satisfactory results for models used in this study when compared with experimental results.

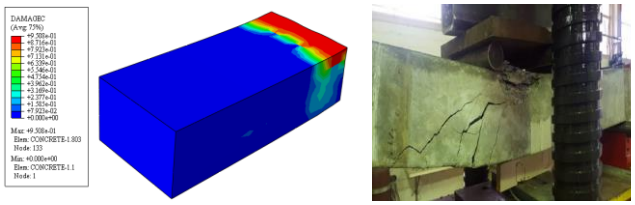

Fig. 10: Comparison of compressive damage for GFRP-RC beam (GB1-1.434-F) based on (a) FE and (b) experimental results[39]

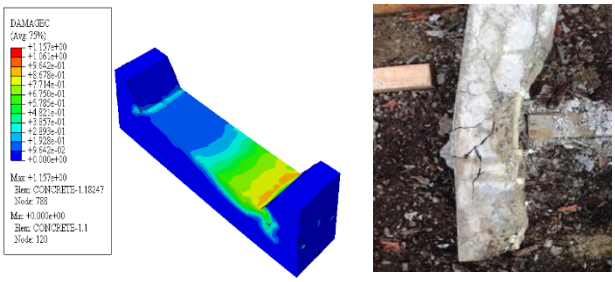

(a) (b)

Fig. 11: Comparison of compressive damage for the column with small eccentricity (GC1-1.434-25) based on (a) FE and (b) experimental results[39]

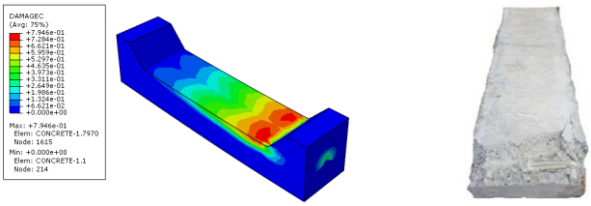

(a) (b)

Fig. 12: Comparison of compressive damage for the column with large eccentricity (GC1-1.434-45) based on (a) FE and (b) experimental results[39]

5. Models built in software

3.2 Material Modelling

In order to investigate the effect of GFRP compressive bars on the flexural strength and ductility of GFRP reinforced concrete beams, and the contribution of GFRP longitudinal bars on the capacity of reinforced concrete columns, 20 concrete column and beam specimens are modelled in the software. Two parameters including compressive reinforcement ratio and ($\frac{\rho}{\rho_{fb}}$) are considered as variables in the specimens built in this section. According to ACI440.1R-15, the flexural capacity of GFRP reinforced beams is dependent on two failure modes, compressive crushing of concrete and FRP rupture. The controlling limit state is determined by comparing FRP reinforcement ratio to the balance reinforcement ratio ($\frac{\rho}{\rho_{fb}}$). The balanced FRP reinforcement ratio is defined in Eq. (21)

$$\rho_{fb} = 0.85\beta_1 \frac{f_c'}{f_{fu}} \frac{E_f\,\varepsilon_{cu}}{E_f\,\varepsilon_{cu} + f_{fu}} \qquad (21)$$

Where f_{fu} represents tensile strength of FRP bars, E_f is the design elasticity modulus of FRP, ε_{cu} is ultimate strain in concrete, and ρ_{fb} indicates FRP reinforcement ratio producing balanced strain conditions.

The amounts of FRP reinforcement ratio are selected by dividing the flexural section into three separate regions according to ACI440.1R-15 [9]: (1) tension-controlled ($\rho < \rho_{fb}$), (2) transition zone ($\rho_{fb} < \rho < 1.4\,\rho_{fb}$), (3) compression-controlled ($\rho > 1.4\,\rho_{fb}$); then by varying the compressive reinforcement ratio from 0 to the amount equal to the FRP reinforcement ratio (ρ), the load-displacement curves are determined. The load-deflection curves of GFRP-reinforced beams for different compressive reinforcement ratios are compared in Fig. 13 and will be explained in the following paragraphs.

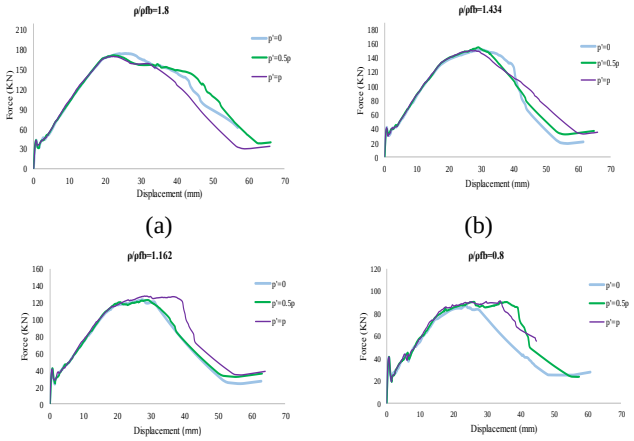

(a) (b)

(c) (d)

Fig. 13: Comparison of load-deflection curves of GFRP reinforced concrete beams for (a) $\frac{\rho}{\rho_{fb}}$=1.8, (b) $\frac{\rho}{\rho_{fb}}$=1.434, (c) $\frac{\rho}{\rho_{fb}}$ =1.162, and (d) $\frac{\rho}{\rho_{fb}}$=0.8.

In all GFRP-RC beams classified into different zones of FRP reinforcement, increasing the compressive reinforcement ratio ($\acute{\rho}$) leads to limited increase in flexural strength and the ductility of beams, especially for beams with $\frac{\rho}{\rho_{fb}} < 1.8$. Also, the pre-peak region is entirely overlapped in all the beam specimens. In cases where the compression reinforcement ratio is equal to FRP reinforcement ratio ($\acute{\rho} = \rho$), decreasing FRP reinforcement ratio to less than the balanced reinforcement ratio, i.e. ($\frac{\rho}{\rho_{fb}}$) from 1.8 to 0.8, results in 46.15% loss in flexural strength, while in cases where the compression reinforcement ratio is half of the FRP reinforcement ratio ($\acute{\rho} = 0.5\rho$) the loss of strength is 47.38% , and, finally, in cases without compression reinforcement ($\acute{\rho} = 0$), the strength loss is equal to 50.24%. The results indicate that decreasing the volume ratio of reinforcement, besides decreasing ($\frac{\rho}{\rho_{fb}}$) results in further loss of flexural strength. The maximum stress contour of some of the beam models built in the software are shown in Fig. 14.

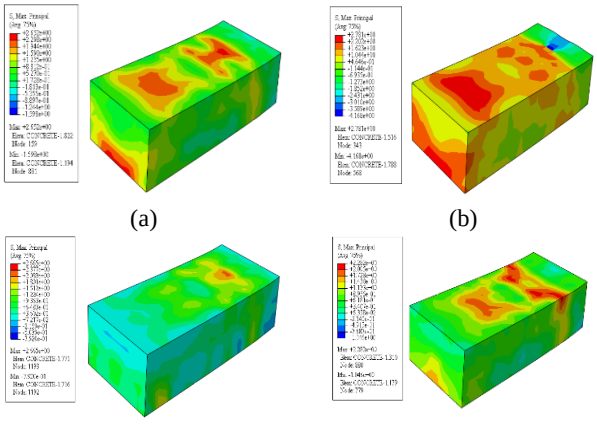

Fig. 14: The maximum stress contours based on FE results of GFRP reinforced beams for (a) $\acute{\rho}=0$, $\frac{\rho}{\rho_{fb}}$=1.8 (b) $\acute{\rho}=0$, $\frac{\rho}{\rho_{fb}}$=1.434 (c) $\rho=\acute{\rho}$, $\frac{\rho}{\rho_{fb}}$=1.162 (d) $\acute{\rho}=0.5*\rho$, $\frac{\rho}{\rho_{fb}}$=0.8.

Fig. 15 shows damage contour of GFRP-RC beam, induced from FEA results, for $\frac{\rho}{\rho_{fb}}$ =1.434 with different compressive reinforcement ratios ($\acute{\rho}$). According to Fig. 15 the increase in compressive reinforcement ratio is followed with a more compressive damage in the middle of the beam span. This is also confirmed by using the curves presented in Fig. **13**, that increasing compressive reinforcement ratios led to increasing the ductility of specimens, and in turn, increasing the strain and the number of cracks on specimen's surface.

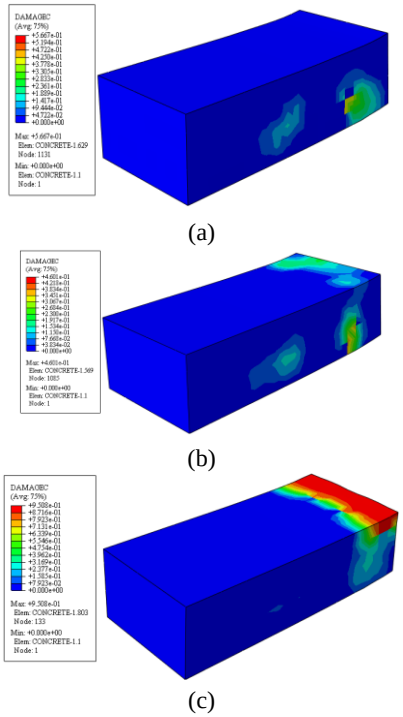

Fig. 15: The damage contours in compression based on FE results for GFRP reinforced beams with $\frac{\rho}{\rho_{fb}}$=1.434 and (a) $\acute{\rho}=0$, (b) $\acute{\rho}=0.5*\rho$, (c) $\rho=\acute{\rho}$.

As shown in Fig. 16, in all the eccentrically loaded columns, the linear region existing in load-displacement curve has been overlapped and the variations are visibly initiated near the peak point. Fig. 16 illustrates that decreasing FRP reinforcement ratio to less than the balanced reinforcement ratio, i.e., ($\frac{\rho}{\rho_{fb}}$) from 1.8 to 0.8, results in the loss in column strength, which is lower compared to the loss in beams. Besides, the amount of loss is slightly higher for columns loaded at higher eccentricity (45mm). For the columns loaded at eccentricities of 25mm and 45mm, the loss in strength is generally equal to 6.2% and 10%, respectively. Also, according to above curves, the columns with smaller ($\frac{\rho}{\rho_{fb}}$) have lower ductility; the reduction of which is more obvious for columns loaded at higher eccentricity (45mm). The damage contours for some of the column models generated in the software are shown in Fig. **17** and Fig. **18**. As observed, the increase in FRP reinforcement ratio to the balance reinforcement ratio ($\frac{\rho}{\rho_{fb}}$) is followed with more damage and crushing in the compression face of eccentrically loaded columns at the same load state.

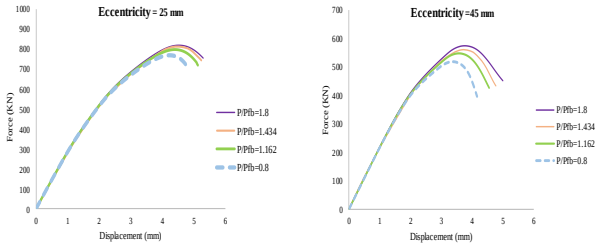

Fig. 16: Comparison of load-displacement curves of GFRP reinforced columns with different eccentricities for variable $\frac{\rho}{\rho_{fb}}$.

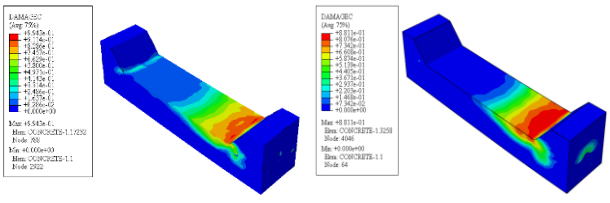

Fig. 17: The damage contours based on FE results for (a) GC1-0.8-25 (b) GC1-1.162-25

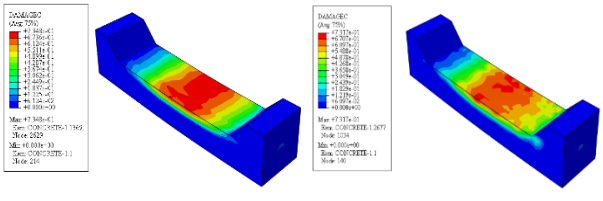

Fig. 18: The damage contours based on FE results for (a) GC1-1.8-45 (b) GC1-0.8-45

6. Interaction Diagram

The axial compression-moment (N-M) interaction diagram represents the axial loading capacity of structural members, especially columns subjected to a bending moment under different eccentricities. The N-M interaction diagrams are applicable for design purposes and indicate the relationship between the axial load and moment of column. The column member analysis is considered safe from the design viewpoint when the load combination falls inside the interaction curve and indicates unsafe design for the load combination outside the interaction curve. Only a few researchers have investigated the relationship between axial compression load and moment of GFRP RC columns using N-M interaction diagrams. Fig. 19 demonstrates the axial compression load-moment interaction diagrams for concrete columns with different proportions of FRP reinforcement to balanced reinforcement ($\frac{\rho}{\rho_{fb}}$). The column loaded concentrically and those with small eccentricities (smaller than e_b) have a slight difference in the N-M diagram obtained experimentally as shown in Fig. **19** (b); while the most discrepancy is observed in columns loaded at higher eccentricity (45mm), that is the result of premature failures due to opening of the lapped stirrups. In general, the N-M interaction diagrams of GFRP-RC columns have a close agreement with the measured curve from the experiment. Fig. 19 (a) to (d) present the N-M interaction diagrams for various longitudinal reinforcement ratios.

According to Fig. **20**, by decreasing ($\frac{\rho}{\rho_{fb}}$) from 1.8 to 0.8, the moment interaction diagram becomes smaller and indicates strength loss. By increasing the reinforcement ratio from 0.8 to 1.8, the increase in load carrying capacity in concentric loading is 3.4%, at peak of bending capacity is 25% and in pure flexure is 46%, indicating that GFRP is most effective when utilized in structural members under mainly bending load.

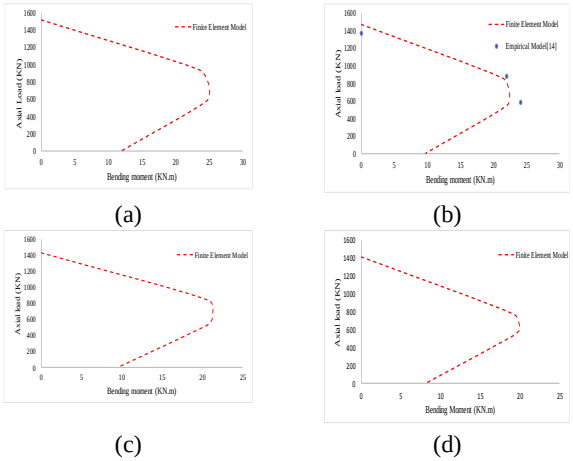

Fig. 19: Axial load-Moment interaction diagrams of GFRP reinforced column (a) $\frac{\rho}{\rho_{fb}} = 1.8$ (b) $\frac{\rho}{\rho_{fb}} 1.434$ (c) $\frac{\rho}{\rho_{fb}} = 1.162$ (d) $\frac{\rho}{\rho_{fb}} = 0.8$.

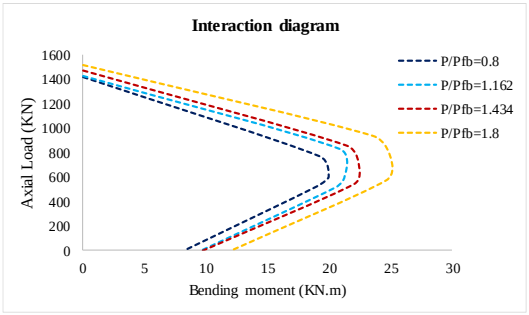

Fig. 20: Influence of longitudinal reinforcement ratio on the Axial Load-Moment interaction diagrams of GFRP reinforced columns.

7. Conclusion

In this paper, the finite element analysis was carried out to predict the behaviour of concrete members reinforced with GFRP bars. After validation of numerical analysis with experimental data, the effect of GFRP compressive reinforcement on the flexural strength and ductility of GFRP-RC beams, and also the contribution of GFRP longitudinal bars on the capacity of RC columns were investigated. Finally, the moment interaction diagrams of both the analysis and tests were presented, and compared with each other. The following conclusions are drawn based on the results:

- Decreasing FRP reinforcement ratio to lower than the balanced reinforcement ratio from 1.8 to 0.8, reduced both the average flexural capacity and the ductility of GFRP-RC beams.
- Change in the compressive reinforcement ratio did not significantly influence the pre-peak region of the load-deflection curve, and a minor effect was observed after peak load. The increase in compressive reinforcement ratio from zero to the amount equivalent to FRP reinforcement ratio did not result in considerable effect on the flexural strength of beams, nevertheless, it led to ductility increase in some cases.
- The FE models predicted the behaviour of experimental column specimens and the slight discrepancy observed is mainly caused by the premature failure due to opening of the lapped stirrups of test specimens. Also, the damage contours achieved through FE simulation had good concordance with experimental results.
- Decreasing FRP reinforcement ratio to lower than the balanced reinforcement ratio from 1.8 to 0.8, decreased the strength up to 6.2% and 10% for columns loaded at 25mm and 45mm eccentricities, respectively. Also, the columns with smaller GFRP longitudinal reinforcement had lower ductility. However, this reduction was significant in the columns loaded at higher eccentricity (45mm).

- The peak load for GFRP-RC beams was slightly overestimated by the FE analysis and provided some deformation in the post-peak collapse region that led to higher ductility. Also, the damage contours properly showed concrete crushing state when compared with experimental results.
- A close agreement was observed between experimental and numerical N-M interaction diagrams, while the most discrepancy was observed at high eccentricity. In addition, decreasing reinforcement ratio with respect to balanced ratio from 1.8 to 0.8 made the N-M diagram smaller, resulting in strength loss of GFRP-RC column. The N-M diagram indicates that GFRP is the most effective when utilized in structural members under mainly bending load.

References:

[1] A. Nanni, A. De Luca, and H. Zadeh, *Reinforced Concrete with FRP Bars: Mechanics and Design*. 2014.

[2] J. Brown and A. T. Consulting, "The Study of FRP Strengthening of Concrete Structures to Increase the Serviceable Design Life in Corrosive Environments," *Struct. Eng.*, 2012.

[3] H. J. Zadeh and A. Nanni, "Design of RC columns using glass FRP reinforcement," *J. Compos. Constr.*, vol. 17, no. 3, pp. 294–304, 2013, doi: 10.1061/(ASCE)CC.1943-5614.0000354.

[4] M. E. Sarafraz, "Flexural Strengthening of RC Columns with Low Longitudinal Steel Ratio using GFRP Bars," *Int. J. Concr. Struct. Mater.*, 2019, doi: 10.1186/s40069-019-0354-z.

[5] N. Kabashi, C. Krasniqi, J. Sustersic, and A. Dautaj, "Flexural Behavior and Cracks in Concrete Beams Reinforced with GFRP Bars," *Int. Congr. Polym. Concr.*, no. Icpic, pp. 617–625, 2018, doi: 10.1007/978-3-319-78175-4.

[6] C. Miàs, L. Torres, A. Turon, M. Baena, I. Vilanova, and M. Llorens, "Experimental Study of Time-dependent Behaviour of Concrete Members Reinforced with GFRP Bars," in *Advances in FRP Composites in Civil Engineering*, 2011, pp. 352–355.

[7] Z. Saleh, M. N. Sheikh, A. M. Remennikov, and A. Basu, "Response of Concrete Beams Reinforced with GFRP Bars Under Static Loads," in *25th Australasian Conference on Mechanics of Structures and Materials*, pp. 765–774.

[8] Z. Saleh, M. N. Sheikh, A. M. Remennikov, and A. Basu, "Response of Concrete Beams Reinforced with GFRP Bars Under Impact Loads," in *25th Australasian Conference on Mechanics of Structures and Materials*, 2020, vol. 37.

[9] ACI 440.1R-15, *Guide for the Design and Construction of Structural Concrete Reinforced with Firber-Reinforced Polymer (FRP) Bars (ACI440.1R-15)*, vol. 22, no. 4. 2015.

[10] S806-02, *Design and Construction of Building Components with Fibre-Reinforced Polymers (CAN/CSA S806-02)*. 2009.

[11] P. D. O. C. Arya, J.L.Clarke, E.A. Kay, "TR 55 : Design guidance for strengthening concrete structures using fiber composite materials," *Struct. Eng. Mech. Comput.*, vol. 2, pp. 1243–1250, 2001.

[12] ISO10406-1, *Iso 10406-1 "Fibre-reinforced polymer (FRP) reinforcement of concrete - Test Methods, Part 1: FRP bars and grids."* 2008.

[13] fib TG 9.3, *fib Bulletin 40: FRP reinforcement in RC structures*, no. 1997. 2002.

[14] M. Elchalakani, A. Karrech, M. Dong, M. S. Mohamed Ali, and B. Yang, "Experiments and Finite Element Analysis of GFRP Reinforced Geopolymer Concrete Rectangular Columns Subjected to Concentric and Eccentric Axial Loading," *Structures*, vol. 14, no. 2017, pp. 273–289, 2018, doi: 10.1016/j.istruc.2018.04.001.

[15] G. B. Maranan, A. C. Manalo, B. Benmokrane, W. Karunasena, and P. Mendis, "Evaluation of the flexural strength and serviceability of geopolymer concrete beams reinforced with glass-fibre-reinforced polymer (GFRP) bars," *Eng. Struct.*, vol. 101, pp. 529–541, 2015, doi: 10.1016/j.engstruct.2015.08.003.

[16] H. Tobbi, A. S. Farghaly, and B. Benmokrane, "Behavior of concentrically loaded fiber-reinforced polymer reinforced concrete columns with varying reinforcement types and ratios," *ACI Struct. J.*, vol. 111, no. 2, pp. 375–385, 2014, doi: 10.14359/51686528.

[17] D. H. Deitz, I. E. Harik, M. Asce, H. Gesund, and F. Asce, "Physical Properties of Glass Fiber Reinforced Polymer Rebars in Compression," *J. Compos. Constr.*, vol. 7, no. 4, pp. 363–366, 2003, doi: https://doi.org/10.1061/(ASCE)1090-0268(2003)7:4(363).

[18] M. Z. Afifi, H. M. Mohamed, and B. Benmokrane, "Axial Capacity of Circular Concrete Columns Reinforced with GFRP Bars and Spirals," *J. Compos. Constr.*, vol. 18, no. 1, p. 04013017, 2014, doi: 10.1061/(ASCE)CC.1943-5614.0000438.

[19] M. Z. Afifi, H. M. Mohamed, and B. Benmokrane, "Strength and Axial Behavior of Circular Concrete Columns Reinforced with CFRP Bars and Spirals," *J. Compos. Constr.*, vol. 18, no. 2, p. 04013035, Apr. 2014, doi: 10.1061/(ASCE)CC.1943-5614.0000430.

[20] Z. Guri and M. Misini, "Experimental and numerical study of circular columns reinforced with steel and GFRP bars," *Mag. Concr. Res.*, pp. 1–27, 2019, doi: 10.1680/jmacr.19.00003.

[21] A. De Luca, F. Matta, and A. Nanni, "Behavior of full-scale glass fiber-reinforced polymer reinforced concrete columns under axial load," *ACI Struct. J.*, vol. 107, no. 5, pp. 589–596, 2010, doi: 10.14359/51663912.

[22] M. Ahmadi, M. Naghipour, and M. Nematzadeh, "Numerical and Experimental Investigations on the Behavior of Steel-reinforced Concrete Columns Subjected to Eccentric Loading," *Int. J. Eng.*, vol. 33, no. 8, pp. 1529–1543, 2020.

[23] M. Alsayed, SH and Al-Salloum, YA and Almusallam, TH and Amjad, "Concrete columns reinforced by glass fiber reinforced polymer rods," *Spec. Publ.*, vol. 188, pp. 103--112, 1999.

[24] X. C. A Mirmiran, W Yuan, "Design for slenderness in concrete columns internally reinforced with fiber-reinforced polymer bars," *ACI Struct. J.*, vol. 98, pp. 116–125, 2001.

[25] C. C. Choo, I. E. Harik, and H. Gesund, "Minimum reinforcement ratio for fiber-reinforced polymer reinforced concrete rectangular columns," *ACI Struct. J.*, vol. 103, no. 3, pp. 460–466, 2006, doi: 10.14359/15325.

[26] U. K. Sharma, P. Bhargava, and S. K. Kaushik, "Behavior of Confined High Strength Concrete Columns under Axial Compression," *J. Adv. Concr. Technol.*, vol. 3, no. 2, pp.

267–281, 2005, doi: 10.3151/jact.3.267.

[27] H. Karim, M. N. Sheikh, and M. N. S. Hadi, "Axial load-axial deformation behaviour of circular concrete columns reinforced with GFRP bars and helices," *Constr. Build. Mater.*, vol. 112, pp. 1147–1157, 2016, doi: 10.1016/j.conbuildmat.2016.02.219.

[28] G. B. Maranan, A. C. Manalo, B. Benmokrane, W. Karunasena, and P. Mendis, "Behavior of concentrically loaded geopolymer-concrete circular columns reinforced longitudinally and transversely with GFRP bars," *Eng. Struct.*, vol. 117, pp. 422–436, 2016, doi: 10.1016/j.engstruct.2016.03.036.

[29] N. Azlina, A. Hamid, A. Ibrahim, R. Thamrin, and H. A. Hamid, "Effect of Longitudinal Reinforcement Ratio on Shear Capacity of Concrete Beams with GFRP Bars," in *International Congress on Polymers in Concrete*, 2018, pp. 617–625, doi: 10.1007/978-981-10-0155-0.

[30] M. Elchalakani, G. Ma, F. Aslani, and W. Duan, "Design of GFRP-reinforced rectangular concrete columns under eccentric axial loading," *Mag. Concr. Res.*, vol. 69, no. 17, pp. 865–877, 2017, doi: 10.1680/jmacr.16.00437.

[31] M. Elchalakani, A. Karrech, M. Dong, M. S. Mohamed Ali, G. (Kevin) Li, and B. Yang, "Testing and modelling of geopolymer concrete members with fibreglass reinforcement," *Proc. Inst. Civ. Eng. - Struct. Build.*, pp. 1–16, 2019, doi: 10.1680/jstbu.18.00173.

[32] T. Yu, J. G. Teng, Y. L. Wong, and S. L. Dong, "Finite element modeling of confined concrete-II: Plastic-damage model," *Eng. Struct.*, vol. 32, no. 3, pp. 680–691, 2010, doi: 10.1016/j.engstruct.2009.11.013.

[33] J. G. Teng, Q. G. Xiao, T. Yu, and L. Lam, "Three-dimensional finite element analysis of reinforced concrete columns with FRP and/or steel confinement," *Eng. Struct.*, vol. 97, pp. 15–28, 2015, doi: 10.1016/j.engstruct.2015.03.030.

[34] H. Mostafaei, M. Ghamami, and P. Aghabozorgi, "Modal identification of concrete arch dam by fully automated operational modal identification," *Structures*, vol. 32, no. August 2020, pp. 228–236, 2021, doi: 10.1016/j.istruc.2021.03.028.

[35] A. M. Amiri, A. Olfati, S. Najjar, P. Beiranvand, and M. H. N. Fard, "Study on Flexural of Reinforced Geopolymer Concrete Beam," *Adv. Sci. Technol. Res. J.*, vol. 10, no. 30, pp. 89–95, 2016, doi: 10.12913/22998624/62630.

[36] A. M. A. Ibrahim, M. F. M. Fahmy, and Z. Wu, "3D finite element modeling of bond-controlled behavior of steel and basalt FRP-reinforced concrete square bridge columns under lateral loading," *Compos. Struct.*, vol. 143, pp. 33–52, 2016, doi: 10.1016/j.compstruct.2016.01.014.

[37] M. Aliasghar-Mamaghani and A. Khaloo, "Seismic behavior of concrete moment frame reinforced with GFRP bars," *Compos. Part B Eng.*, vol. 163, no. September 2018, pp. 324–338, 2019, doi: 10.1016/j.compositesb.2018.10.082.

[38] H. Sadraie, A. Khaloo, and H. Soltani, "Dynamic performance of concrete slabs reinforced with steel and GFRP bars under impact loading," *Eng. Struct.*, vol. 191, no. December 2018, pp. 62–81, 2019, doi: 10.1016/j.engstruct.2019.04.038.

[39] M. Elchalakani and G. Ma, "Tests of glass fibre reinforced polymer rectangular concrete columns subjected to concentric and eccentric axial loading," *Eng. Struct.*, vol. 151, pp. 93–104, 2017, doi: 10.1016/j.engstruct.2017.08.023.

[40] M. N. S. Hadi, F. Asce, and J. Youssef, "Experimental Investigation of GFRP-Reinforced and GFRP-Encased Square Concrete Specimens under Axial and Eccentric Load , and Four-Point Bending Test," *J. Compos. Constr.*, vol. 20, no. 5, pp. 1–16, 2016, doi: 10.1061/(ASCE)CC.1943-5614.0000675.

[41] M. N. S. Hadi, F. Asce, H. Karim, and M. N. Sheikh, "Experimental Investigations on Circular Concrete Columns Reinforced with GFRP Bars and Helices under Different Loading Conditions," *J. Compos. Constr.*, vol. 20, no. 4, pp. 1–12, 2016, doi: 10.1061/(ASCE)CC.1943-5614.0000670.

[42] Pultrall. V-Rod Specification:, *composite reinforcing rods technical data sheet. Canada: Thetford Mines*, vol. 2. 2012.

[43] C. Z. Liu W, Xu M, "Parameters calibration and verification of concrete damage plasticity model of Abaqus.," *J. Compos. Constr.*, vol. 19, no. 1, Feb. 2014, doi: 10.1061/(ASCE)CC.1943-5614.0000482.

[44] H. Mostafaei and F. Behnamfar, "Effect of the vertical earthquake component on nonlinear behavior of an arch dam having a foundation with discontinuities," *Int. J. Numer. methods Civ. Eng.*, vol. 4, no. 2, pp. 69–78, 2019.

[45] H. Mostafaei, F. Behnamfar, and M. Alembagheri, "Nonlinear analysis of stability of rock wedges in the abutments of an arch dam due to seismic loading," *Struct. Monit. Maint.*, vol. 7, no. 4, pp. 295–317, 2020.

[46] ACI 363, *State-of-the-Art Report on High-Strength Concrete (ACI 363R-92).*, vol. 92. 1992.

[47] M. Elchalakani, A. Karrech, M. F. Hassanein, and B. Yang, "Plastic and yield slenderness limits for circular concrete filled tubes subjected to static pure bending," *Thin-Walled Struct.*, vol. 109, pp. 50–64, 2016, doi: 10.1016/j.tws.2016.09.012.

[48] A. Karrech, T. Poulet, and K. Regenauer-Lieb, "A limit analysis approach to derive a thermodynamic damage potential for non-linear geomaterials," *Philos. Mag.*, vol. 92, no. 28–30, pp. 3439–3450, 2012, doi: 10.1080/14786435.2012.687469.

[49] A. I. Karabinis and T. C. Rousakis, "Concrete confined by FRP material: A plasticity approach," *Eng. Struct.*, vol. 24, no. 7, pp. 923–932, 2002, doi: 10.1016/S0141-0296(02)00011-1.

[50] A. Karrech, F. Abbassi, H. Basarir, and M. Attar, "Self-consistent fractal damage of natural geo-materials in finite strain," *Mech. Mater.*, vol. 104, pp. 107–120, 2017, doi: 10.1016/j.mechmat.2016.08.017.

[51] W. Ren, L. H. Sneed, Y. Yang, and R. He, "Numerical Simulation of Prestressed Precast Concrete Bridge Deck Panels Using Damage Plasticity Model," *Int. J. Concr. Struct. Mater.*, vol. 9, no. 1, pp. 45–54, 2015, doi: 10.1007/s40069-014-0091-2.

[52] J. B. Mander, M. J. N. Priestley, and R. Park, "Theoretical Stress-Strain Model for Confined Concrete," *J. Struct. Eng.*, vol. 114, no. 8, pp. 1804–1826, Sep. 1988, doi: 10.1061/(ASCE)0733-9445(1988)114:8(1804).

[53] A. J. Kappos and D. Konstantinidis, "Statistical analysis of confined high strength concrete," *Mater. Struct.*, vol. 32, no. 10, pp. 734–748, 2018, doi: 10.1007/bf02905070.

[54] AS3600, *AS 3600-2009: Concrete Structures, Australian Standard. Sydney, Australia:* Australian Standard, 2009, p. 208.

[55] J. Stoner, "Finite Element Modelling of GFRP Reinforced Concrete Beams," University of Waterloo, 2015.

[56] D. Kent and R. P. Division, "Flexural members with confined concrete," *J. Struct. Div.*, 1971.